RESEARCH ARTICLE

Closed-Loop Soft Starter Firing Angle Control Method Using Only Current Feedback

DAE-YOUNG YANG [ID][1], YOUNG-SEOK KIM [ID][1], TAE-HO OH [ID][1],
SANG-HOON LEE [ID][2], (Member, IEEE), AND DONG-IL CHO [ID][1,2], (Member, IEEE)
[1]Department of Electrical and Computer Engineering, Institute of Engineering Research, Seoul National University, Seoul 08826, South Korea
[2]Research and Development Center, RS Automation Company Ltd., Pyeongtaek 17709, South Korea

Corresponding author: Dong-Il Cho (dicho@snu.ac.kr)

ABSTRACT A soft starter is commonly utilized in various industrial induction motor systems to reduce the inrush current during motor startup. The conventional voltage ramp-up method, used in the typical soft starter, gradually increases the voltage over the startup period. However, this method can result in a significant voltage increase as the induction motor approaches its rated speed, resulting in a rapid torque increase compared to the beginning part of the startup phase. This sudden torque increase can potentially cause physical damage to the induction motor system due to a transient current overshoot, which in turn can result in resonance. Additionally, the changes in the parameters of the induction motors can lead to the variations in torque during startup, especially because of the air gap permeance. Therefore, a firing angle control method for the soft starter that maintains a constant torque, facilitating a gradual increase in speed, is desirable. This paper proposes a novel firing angle control method, to achieve a constant torque and a gradual speed increase, using only current feedback. This paper is the first time that a change in air gap permeance is considered and compensated for in controlling the firing angle of the soft starter. The air gap permeance variation is modeled as an effective inertia in the transient response of the induction motor. Experimental results demonstrate that the proposed method effectively reduces rapid torque increases and speed variations compared to the conventional voltage ramp-up method, through its application to a 30kW industrial induction motor system.

INDEX TERMS Induction motors, thyristors, air gaps, current control.

I. INTRODUCTION

In recent years, the demand for motors in industrial applications has been driven by the need for increased automation, stricter energy efficiency regulations, and a shift toward sustainable manufacturing practices. These developments have been accelerating the adoption of high-efficiency electric power systems, including motors, across various industries. Among the different types of industrial electric motors, induction motors are particularly significant, accounting for about 60% of all motors. Their simplicity, robustness, and high energy efficiency make them indispensable in a wide range of industrial applications. Consequently, induction

motors have become an important research topic within industrial engineering [1], [2], [3]. However, the startup phase presents a notable remarkable challenge, primarily due to the inrush current that can shoot up to 6 to 8 times the motor's rated current, which presents risks to electrical components due to thermal and mechanical stress and affects the overall stability of the system. This surge, caused by the speed difference between the stator and the rotor's magnetic field, must be addressed to ensure the motor's stable startup [4]. Furthermore, the inrush current presents a risk to electrical components due to thermal and mechanical stress and affects the overall stability of the system.

To overcome these challenges, soft starters composed of thyristors that control the current and voltage supplied to an induction motor have been commonly used. They were

The associate editor coordinating the review of this manuscript and approving it for publication was Yuh-Shyan Hwang [ID].

essential in various industrial equipment to mitigate inrush current, extend the lifespan of induction motors, and stabilize systems, offering cost-effective solutions with excellent energy efficiency. This is beneficial for applications involving constant-speed operations, such as fans, conveyor belts, and other industrial induction motor applications. Employing a soft starter with a delta-connected induction motor, which integrates parallel resistors in a delta-connected configuration, necessitates the development of tailored control strategies [5], [6], [7]. Traditionally, the voltage magnitude across the thyristor is managed by adjusting the duration during which the thyristor is not conducting, a method known as firing angle (alpha) control. Advances in this area have led to the development of the alpha + gamma control method, which additionally controls the zero-crossing time of the current to mitigate rapid torque increases when the motor reaches its rated speed. Despite these advancements, challenges remain with the voltage ramp-up method, which involves a linear increase in the firing angle of the thyristors to mitigate the inrush current. Particularly as the motor reaches its rated speed, this method leads to a rapid increase in both voltage magnitude and torque, potentially critical issues [8]. To overcome these effects, a current-limiting method is proposed, utilizing current feedback from the soft starter to control the firing angle and prevent excessive voltage escalation [9]. This method has proven to be effective in reducing high torque compared to the voltage ramp-up method. However, the challenge of a rapid increase in speed due to a torque increase arises when the rated speed is reached. Recently, the voltage ramp-up method and the current limit method have become conventional control methods for soft starters in industrial applications.

To improve the cost-effectiveness of soft starters, 2-phase soft starters and their control methods were introduced. Control methods were designed to balance the currents in the two controlled phases during startup [10], [11]. This approach includes a PI controller with a firing angle control method using current feedback and an open-loop firing angle control method. The efficiency of the two-phase soft starter was enhanced with fewer thyristor elements, but the issue of torque oscillation remains unresolved. In a conventional 3-phase soft starter, various control methods were developed for firing angle control. A current limit control method using a PI controller was proposed, with the PI gain selected through the optimization algorithm of the flower pollination algorithm (FPA) [12]. Another proposed method involves an artificial neural network-based firing angle control and an offline tuning approach, utilizing voltage and current data to control the acceleration of the induction motor during startup [13]. Moreover, firing angle control methods were developed to mitigate energy dissipation during the startup phase [14], [15]. These techniques aimed to estimate flux and torque within the induction motor during startup by using voltage and current data. Their main objective was to reduce the operational duration of the thyristor to diminish energy consumption until

the motor reached its rated speed. However, it's noteworthy that these methods result in discontinuous thyristor operation, including speed variations and torque oscillations. Therefore, controlling speed and torque during the startup of an induction motor using a soft starter requires either an additional sensor or an offline algorithmic calculation process. Furthermore, the startup control of induction motors is complicated by variations in air gap permeance, a phenomenon that significantly influences motor performance [16]. These variations can introduce additional complexities in managing the inrush current and achieving stable motor operation. Thus, there is a need for detailed modeling and a control method that specifically addresses the changes in air gap permeance during the motor's startup phase. However, existing control methods for soft starters have not incorporated modeling of air gap permeance, nor have they proposed control strategies that take these variations into account. Also, controlling speed and torque during the startup of an induction motor with a soft starter typically requires additional sensors or an offline algorithmic calculation process.

This paper proposes a novel firing angle control method for soft starters, particularly designed to compensate for the changes in air gap permeance for the first time. The startup of the induction motor exhibits transient responses. To analyze these responses, this paper employs a bond graph modeling method to represent the induction motor and soft starter, as detailed in Session II. This modeling approach analyzes the influence of changes in the air gap on torque, aiming to maintain a gradual speed increase. The analysis of the torque of the induction motor, based on changes in the air gap and the firing angle control algorithm to maintain torque considering air gap variations, is presented in Session III. The induction motor with a soft starter system is simulated using MATLAB/SIMULINK. The parameters of the induction motor are estimated from the datasheet of an industrial induction motor to reduce discrepancies between an actual induction motor, as shown in Session IV. Experiments with a 30kW industrial induction motor and a soft starter demonstrate the effectiveness of the proposed method in minimizing torque fluctuations using only current data. The proposed method introduces an approach that adapts to air gap permeance variations, achieving a gradual speed increase through current feedback only for soft starter technology in industrial applications.

II. MODELING OF THE INDUCTION MOTOR SYSTEM

An induction motor comprises multiple energy domains, including electrical, magnetic, and mechanical systems. Typically, induction motors are modeled using electrical circuits where the internal parameters such as stator, rotor, and air gap parameters are assumed to be in the steady state. The conventional single-phase electric circuit model of the induction motor with a soft starter is depicted in Fig. 1. However, during startup, induction motors exhibit transient responses that result in changes in internal parameters. In traditional circuit

models, it is very difficult and not intuitive to effectively identify dependent variables in multiple energy domains. The bond graph method represents a physical dynamic system as a signal-flow graph, describing the flow of energy in terms of effort and flow, where effort represents generalized forces and flow represents generalized velocities or rates of flow. This method is especially suitable for modeling induction motors that have multiple energy domains [17]. Bond-graph modeling allows representing combined electrical, electromagnetic, and mechanical energy domain systems to be effectively modeled. For example, in electrical domain, voltage and current are effort and flow. In mechanical domain, torque and angular speed are effort and flow. In electromagnetic domain, magnetic flux and magnetomotive force are effort and flow. Then, transformers and gyrators are used to represent the energy conversion process. Thus, the multiple domain system can be easily modeled. The differential equation is easily derived and used for designing control laws. Therefore, the bond graph modeling can be effectively utilized for induction motor control, especially during the startup phase when torque and current fluctuations occur. Because an induction motor consists of multi-energy domains, it is difficult to determine the torque-dependent permeance among the various permeances of the induction motor using only circuit diagrams. Therefore, when modeling the induction motor through the bond graph method, torque-dependent energy elements can be intuitively represented and utilized for the control algorithm. Additionally, the air gap permeance is not an independent element; rather, it passes through the gyrator, increasing load inertia. To improve control performance, it is critical to account for these internal parameter changes. In this session, the induction motor is modeled using the bond graph method. In this paper, the effect of air gap variations in induction motors on torque during startup is analyzed using bond graph modeling. An induction motor modeled with a bond graph is divided into five main parts: Input voltage & soft starter, stator, rotor, air gap, and shaft.
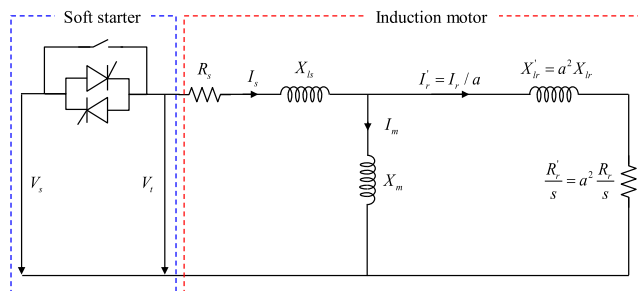

FIGURE 1. Conventional single-phase electric circuit model of the induction motor with a soft starter.

A. INPUT VOLTAGE & SOFT STARTER

The input voltage & soft starter part is an electrical system and consists of the voltage applied to the induction motor and the soft starter. The phases of the input voltage are determined

by the phase shifter 'PS', and the thyristors of each phase are designated as 'TY'. The input voltage satisfies the following equations:

$$S_e = e_{in}, \tag{1}$$

$$e_i = e_{in} \cdot e^{-j\theta_i}, \tag{2}$$

$$\sum_{i=1}^{\infty} e_i = 0. \tag{3}$$

where e_{in} is the input signal, S_e is the effort source of the bond graph, θ_i is the shift angle, and e_i is the phase-shifted signal.

The U, V, and W phases of the input voltage are phase-shifted by θ_1, θ_2, and θ_3, respectively, before being applied to the soft starter. The thyristor controls the three phases of the input signal. The thyristor operates in two distinct states: conducting and blocking. Upon receiving a gate signal from the thyristor controller, it enters the conducting state. As the current passes the zero-crossing point, it reverts to the blocking state, and no further current flows until the next gate signal is received. The firing angle (α) represents the time between the conducting and blocking states. In the bond graph, the conducting state is represented by V_{on} at w = 1, and the blocking state is represented by V_{off} at w = 0. After the input voltage passes through the thyristors, it is represented by the three phases A, B, and C.

B. STATOR

The stator of an induction motor part is of both the electrical and magnetic systems. The bond graph model of the stator is shown in Fig. 2 (a), with phase A illustrated. When an input signal is applied to the electrical system, it is transformed into the magnetic system through the gyrator, and energy flows into the air gap. In the bond graph, the stator has a resistance (R_{as}), and a permeance ($C_{P,as}$), and its effective winding ratio of the stator is denoted as N_s. The effort (e) and flow (f) equations of the stator in the bond graph are expressed as follows:

$$e_1 = V_{as} = V_m \sin(\omega t), \tag{4}$$

$$e_2 = V_{as} = I_{as}R_{as}, \tag{5}$$

$$e_3 = e_{as} = V_{as} - I_{as}R_{as}, \tag{6}$$

$$e_4 = e_5 = e_6 = N_s I_{as}, \tag{7}$$

$$f_1 = f_2 = f_3 = I_{as}, \tag{8}$$

$$f_4 = \frac{1}{N_s}(V_{as} - I_{as}R_{as}), \tag{9}$$

$$f_5 = \frac{d}{dt}(N_s I_{as} C_{P,as}), \tag{10}$$

$$f_6 = \frac{1}{N_s}(V_{as} - I_{as}R_{as}) - \frac{d}{dt}N_s I_{as} C_{P,as}. \tag{11}$$

where V_{as} is the voltage of the stator, I_{as} is the current of the stator, and V_m is the maximum amplitude of the voltage.

C. ROTOR

The rotor part of an induction motor is also composed of electrical and magnetic structures and is essentially an inverted

form of the stator. The bond graph model of the rotor is shown in Fig. 2 (b), with phase A shown. The energy flows from the air gap to the magnetic system and is transformed into the electrical system through the gyrator. In Fig. 2 (b), the rotor has a permeance ($C_{P,ar}$), and a resistance (R_{ar}), and its effective winding ratio of the rotor is denoted as N_r. The effort and flow equations of the rotor in the bond graph are expressed as follows:

$$f_7 = \frac{1}{N_r}\left(V_{ar} - I_{ar}R_{ar}\right) - \frac{d}{dt}N_r I_{ar}C_{P,ar}, \quad (12)$$

$$f_8 = \frac{d}{dt}\left(N_r I_{ar}C_{P,ar}\right), \quad (13)$$

$$f_9 = \frac{1}{N_r}\left(V_{ar} - I_{ar}R_{ar}\right), \quad (14)$$

$$f_{10} = f_{12} = f_{12} = I_{ar}, \quad (15)$$

$$e_7 = e_8 = e_9 = N_r I_{ar}, \quad (16)$$

$$e_{10} = V_{ar} - I_{ar}R_{ar}, \quad (17)$$

$$e_{11} = V_{ar} = I_{ar}R_{ar}, \quad (18)$$

$$e_{12} = V_{ar} = 0. \quad (19)$$

where I_{ar} is the current of the rotor, and V_{ar} is the voltage of the rotor. Because the rotor is short-circuited, the V_{ar} is always 0.
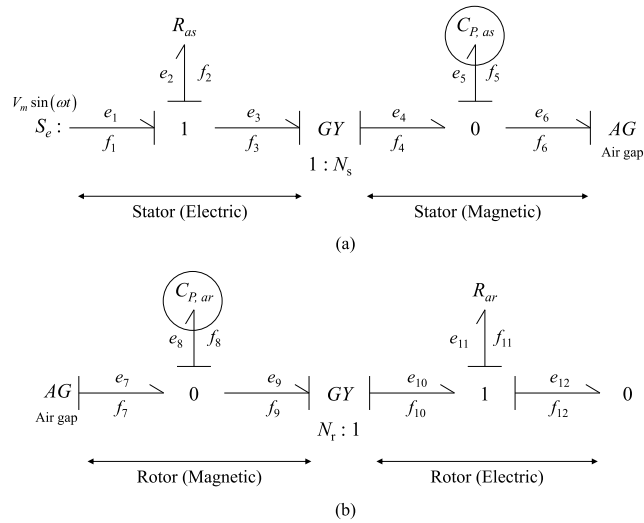

FIGURE 2. (a) Bond graph model of the stator, (b) Bond graph model of the rotor.

D. AIR GAP

The air gap is the space between the stator and rotor, and its size affects the permeance value. During motor startup, the changing magnetic field influences the permeance value of the air gap. Because changes in air gap permeance are critical for the induction motor's torque, it is essential to consider air gap variations when controlling the motor [15], [16]. The bond graph model of the air gap is shown in Fig. 3. The air
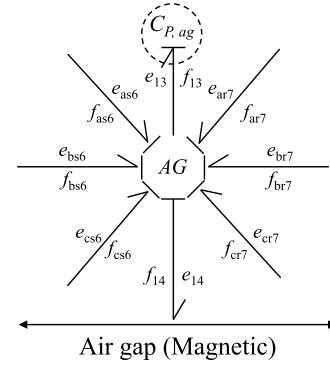

FIGURE 3. Bond graph model of the air gap.

gap satisfies the following equations in the bond graph:

$$f_i = \frac{d}{dt}\left(C_{P,ag}\left(\sum_{k=1}^{6} e_k \left(\sum_{i=1}^{6} \cos\left(\alpha_i - \alpha_k\right)\right)\right)\right), \quad (20)$$

$$P_m = \sum_{k=1}^{\infty} e_k f_k. \quad (21)$$

where $\cos\left(\alpha_i - \alpha_k\right)$ is the spatial angle between the k-th and i-th winding axes, $C_{P,ag}$ is the permeance of the air gap, and P_m is the reactive power. The $C_{P,ag} = C_{P,m} + C_{P,\alpha}$ is divided into air gap mutual inductance ($C_{P,m}$) and air gap variable inductance ($C_{P,\alpha}$).

E. SHAFT

The shaft of the induction motor is a mechanical energy system. The bond graph model of the shaft is shown in Fig. 4. The energy from the air gap flows to the shaft. In Fig. 4, N_P is the number of poles of the induction motor, the shaft has a damper (R_B), shaft inertia is denoted as J, and T_L is a load torque. The effort and flow equations of the shaft in the bond graph are expressed as follows:

$$f_{15} = f_{16} = f_{17} = \omega_r, \quad (22)$$

$$e_{15} = \frac{N_P}{2}f_{14} = T_m, \quad (23)$$

$$e_{16} = \omega_r R_B, \quad (24)$$

$$e_{17} = J\dot{f}_{17} = J\dot{\omega}_r, \quad (25)$$

$$T_m - T_L = \omega_r R_B + J\dot{\omega}_r. \quad (26)$$

where ω_r is the speed of the rotor, and T_m is the motor torque. The f_{14} can be calculated when the motor torque is known using (23). Additionally, from Fig.3, it can be shown that $f_{14} + f_{13}$ represents the sum of the flows of the stator and rotor. Thus, the bond graph model of the induction motor is shown in Fig. 5. The voltage equations of the induction motor model can be expressed in three cases. In Case 1, either two or three thyristors are in a blocking state whereby a magnetic field is not generated in the rotor. As a result, the induction motor is unable to enter the startup. In Case 2, only one phase thyristor is in the blocking state where the magnetic field is generated, and the induction motor can enter

the startup. However, it is worth noting that only two phases are connected to the induction motor at any given point. In Case 3, none of the thyristors are in a blocking state, where three phases are always connected. During the startup of the induction motor, these three cases are generated in turn. The voltage equations for these three phases, derived from bond graph modeling equations (4)-(21), are expressed as follows:

Case 1: Either two or three thyristors are in a blocking state. (Based on A phase)

The voltage equation is calculated as follows:

$$V_{as} = I_{as}R_{as} + \frac{d}{dt}\left(\left(C_{P,as} + C_{P,ag}\right)N_s^2 I_{as}\right)$$
$$= I_{as}R_{as} + \frac{d}{dt}L_{ss}I_{as} = I_{as}R_{as} + \frac{d\Psi_{as}}{dt}. \quad (27)$$

where a magnetic field is not generated, so no energy is transferred to the rotor ($I_{ar} = I_{br} = I_{cr} = 0$).

Case 2: Only one phase thyristor is in the blocking state. (Based on A, and B phases)

The voltage equation is calculated as follows:

$$V_{as} = I_{as}R_{as} + \frac{d}{dt}\left(\left(C_{P,as} + C_{P,ag}\right)N_s^2 I_{as} - \frac{1}{2}C_{P,ag}N_s^2 I_{bs}\right)$$
$$+ \frac{d}{dt}\left(C_{P,ag}\left(N_s N_r I_{ar}\cos\theta\right)\right)$$
$$+ \frac{d}{dt}\left(C_{P,ag}\left(N_s N_r I_{br}\cos\left(\theta + \frac{2}{3}\pi\right)\right)\right)$$
$$+ \frac{d}{dt}\left(C_{P,ag}\left(N_s N_r I_{cr}\cos\left(\theta + \frac{4}{3}\pi\right)\right)\right)$$
$$= I_{as}R_{as} + \frac{d}{dt}\left(L_{ss}I_{as} - \frac{1}{2}L_{ag}I_{bs}\right)$$
$$+ \frac{d}{dt}\left(L_{ag}\left(I_{ar}\cos\theta + I_{br}\cos\left(\theta + \frac{2}{3}\pi\right)\right.\right.$$
$$\left.\left. + I_{cr}\cos\left(\theta + \frac{4}{3}\pi\right)\right)\right)$$
$$= I_{as}R_{as} + \frac{d\Psi_{as}}{dt}, \quad (28)$$

$$V_{bs} = I_{bs}R_{bs} + \frac{d}{dt}\left(\left(C_{P,bs} + C_{P,ag}\right)N_s^2 I_{bs} - \frac{1}{2}C_{P,ag}N_s^2 I_{as}\right)$$
$$+ \frac{d}{dt}\left(C_{P,ag}\left(N_s N_r I_{ar}\cos\left(\theta + \frac{4}{3}\pi\right)\right)\right)$$
$$+ \frac{d}{dt}\left(C_{P,ag}\left(N_s N_r I_{br}\cos\theta\right)\right)$$
$$+ \frac{d}{dt}\left(C_{P,ag}\left(N_s N_r I_{cr}\cos\left(\theta + \frac{2}{3}\pi\right)\right)\right)$$
$$= I_{bs}R_{bs} + \frac{d}{dt}\left(L_{ss}I_{bs} - \frac{1}{2}L_{ag}I_{as}\right)$$
$$+ \frac{d}{dt}\left(L_{ag}\left(I_{ar}\cos\left(\theta + \frac{4}{3}\pi\right)\right.\right.$$
$$\left.\left. + I_{br}\cos\theta + I_{cr}\cos\left(\theta + \frac{2}{3}\pi\right)\right)\right)$$
$$= I_{bs}R_{bs} + \frac{d\Psi_{bs}}{dt}. \quad (29)$$

Case 3: None of the thyristors are in a blocking state (The A and B phases are equal to (28), (29)).

The voltage equation is calculated as follows:

$$V_{cs} = I_{cs}R_{cs} + \frac{d}{dt}\left(\left(C_{P,cs} + C_{P,ag}\right)N_s^2 I_{cs}\right.$$
$$\left. - \frac{1}{2}C_{P,ag}N_s^2\left(I_{as} + I_{bs}\right)\right)$$
$$+ \frac{d}{dt}\left(C_{P,ag}\left(N_s N_r I_{ar}\cos\left(\theta + \frac{2}{3}\pi\right)\right)\right)$$
$$+ \frac{d}{dt}\left(C_{P,ag}\left(N_s N_r I_{br}\cos\left(\theta + \frac{4}{3}\pi\right)\right)\right)$$
$$+ \frac{d}{dt}\left(C_{P,ag}\left(N_s N_r I_{cr}\cos\theta\right)\right)$$
$$= I_{cs}R_{cs} + \frac{d}{dt}\left(L_{ss}I_{cs} - \frac{1}{2}L_{ag}\left(I_{as} + I_{bs}\right)\right)$$
$$+ \frac{d}{dt}\left(L_{ag}\left(I_{ar}\cos\left(\theta + \frac{2}{3}\pi\right) + I_{br}\cos\left(\theta + \frac{4}{3}\pi\right)\right.\right.$$
$$\left.\left. + I_{cr}\cos\theta\right)\right)$$
$$= I_{cs}R_{cs} + \frac{d\Psi_{cs}}{dt}. \quad (30)$$

Hence, the voltage equation of the stator, rotor, and torque equation can be represented as follows:

$$\mathbf{V}_s = \mathbf{I}_s\mathbf{R}_s + \frac{d\Psi_s}{dt}, \quad (31)$$

$$\mathbf{V}_r = \mathbf{I}_r\mathbf{R}_r + \frac{d\Psi_r}{dt}, \quad (32)$$

$$T_m = I_{as}L_{ag}\left[-\sin\theta I_{ar} - \sin\left(\theta + \frac{2}{3}\pi\right)I_{br}\right.$$
$$\left. - \sin\left(\theta - \frac{2}{3}\pi\right)I_{cr}\right]\cdot\frac{N_p}{2}$$
$$+ I_{bs}L_{ag}\left[-\sin\left(\theta - \frac{2}{3}\pi\right)I_{ar} - \sin\theta I_{br}\right.$$
$$\left. - \sin\left(\theta + \frac{2}{3}\pi\right)I_{cr}\right]\cdot\frac{N_p}{2}$$
$$+ I_{cs}L_{ag}\left[-\sin\left(\theta + \frac{2}{3}\pi\right)I_{ar} - \sin\left(\theta - \frac{2}{3}\pi\right)I_{br}\right.$$
$$\left. - \sin\theta I_{cr}\right]\cdot\frac{N_p}{2}, \quad (33)$$

$$J\frac{d\omega}{dt} + R_B\omega = T_m - T_L. \quad (34)$$

where $C_{P,ag}$ is included in the rotor's voltage equation as well as in the stator's voltage equations (27)-(30) and $L_{ag} = N_s N_r C_{P,ag}$ is the inductance of the air gap. For the startup of the induction motor, air gap permeance is one of the most important state variables that influence starting torque. Conventional induction motor modeling methods either neglected the air gap permeance or assumed it to be a constant. Therefore, they did not use the air gap permeance as a state variable when modeling the transient response of the induction motor. In this paper, air gap permeance is modeled as an effective inertia included in the state variables of the induction motor system, which shows the transient response of this system.
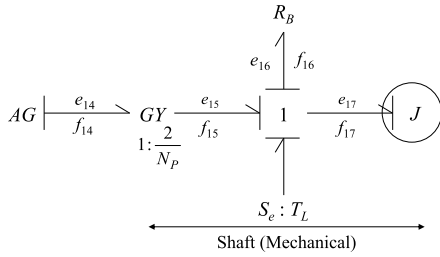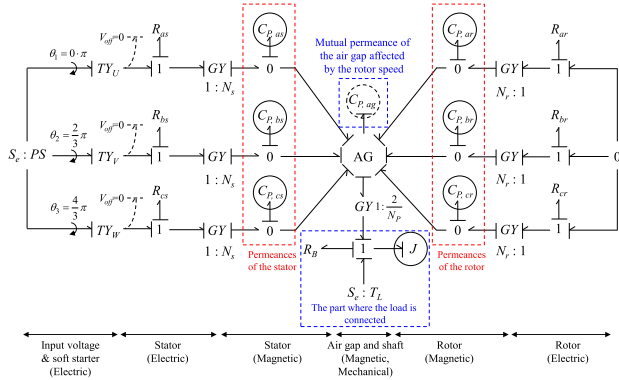
FIGURE 4. Bond graph model of the shaft.

FIGURE 5. Bond graph model of the induction motor.

III. PROPOSED FIRING ANGLE CONTROL METHOD

A. FIRING ANGLE CONTROL METHOD TO MAINTAIN TORQUE

The soft starter regulates the voltage supplied to the induction motor by controlling the firing angle of the thyristor, using current feedback from the induction motor. A representation of the induction motor system under the control of a soft starter with Park (dq) transformation is as follows:

$$\frac{d}{dt}\begin{bmatrix} i_{ds}^s \\ i_{qs}^s \\ \phi_{dr}^s \\ \phi_{qr}^s \end{bmatrix} = \mathbf{A}\begin{bmatrix} i_{ds}^s \\ i_{qs}^s \\ \phi_{dr}^s \\ \phi_{qr}^s \end{bmatrix} + \begin{bmatrix} \frac{1}{\sigma L_{ss}} & \frac{1}{\sigma L_{ss}} & 0 & 0 \end{bmatrix}\begin{bmatrix} V_{ds} \\ V_{qs} \\ 0 \\ 0 \end{bmatrix}. \quad (35)$$

where system matrix

$$\mathbf{A}$$

$$= \begin{bmatrix} R_r\frac{L_{ag}^2}{\sigma L_{ss}L_{sr}^2} - R_s & 0 & R_r\frac{L_{ag}}{\sigma L_{ss}L_{sr}^2} & \frac{L_{ag}}{\sigma L_{ss}L_{sr}}N_P\omega_r \\ 0 & R_r\frac{L_{ag}^2}{\sigma L_{ss}L_{sr}^2} - R_s & \frac{L_{ag}}{\sigma L_{ss}L_{sr}}N_P\omega_r & R_r\frac{L_{ag}}{\sigma L_{ss}L_{sr}^2} \\ \frac{L_{ag}R_r}{L_{sr}} & 0 & -\frac{R_r}{L_{sr}} & -\omega_r \\ 0 & \frac{L_{ag}R_r}{L_{sr}} & -\omega_r & -\frac{R_r}{L_{sr}} \end{bmatrix},$$

$\sigma = 1 - \left(L_{ag}^2/(L_{ss}L_{sr})\right)$, L_{ss} is stator mutual inductance, and L_{sr} is rotor mutual inductance. The dq transformation is used in induction motor control to simplify the analysis and control of induction motors by converting three-phase currents and voltages into a two-axis coordinate system. This transformation allows for easier implementation of control methods, achieving precise torque and speed control. The dq

transformation is expressed as follows:

$$\begin{bmatrix} i_d \\ i_q \end{bmatrix} = \begin{bmatrix} \cos(\theta) & \cos\left(\theta - \frac{2}{3}\pi\right) & \cos\left(\theta + \frac{2}{3}\pi\right) \\ -\sin(\theta) & -\sin\left(\theta - \frac{2}{3}\pi\right) & -\sin\left(\theta + \frac{2}{3}\pi\right) \end{bmatrix}$$
$$\times \begin{bmatrix} i_a \\ i_b \\ i_c \end{bmatrix}. \quad (36)$$

There are two traditional torque control methods for induction motors: direct torque control and indirect torque control. In the direct torque control method, both flux and torque are regulated via the dq current in a coordinate frame synchronized with the flux, provided that the flux position is known [20], [21]. Conversely, the indirect torque control method indirectly regulates the magnitude of the flux and torque by controlling the slip angle speed of the induction motor, assuming the rotor speed is known [22], [23]. However, obtaining speed information for the induction motor, particularly when using a soft starter, is often not traditional. Consequently, this paper proposes a torque control method for soft starters, resembling direct torque control but applicable even when voltage data is unavailable.

The fux equations in a rotational frame with speed(e) can be expressed as:

$$\phi_{dqs}^e = L_s i_{dqs}^e + L_{ag} i_{dqr}^e, \quad (37)$$
$$\phi_{dqr}^e = L_{ag} i_{dqs}^e + L_r i_{dqr}^e. \quad (38)$$

The rotor flux angle (θ_e) can be calculated as follows:

$$\theta_e = \arctan\left(\frac{\phi_{qr}^s}{\phi_{dr}^s}\right). \quad (39)$$

In a rotating coordinate frame rotated by e, because the rotor flux is synchronized to the d-axis, so all rotor flux components will only exist on the d-axis, and the flux on the q-axis will always be zero. So, the rotor voltage equation and rotor flux estimation equation are expressed as follows:

$$0 = R_r i_{dr}^e + \frac{d\phi_{dr}^e}{dt}, \quad (40)$$
$$\phi_{dr}^e = L_{ag} i_{ds}^e + L_r i_{dr}^e. \quad (41)$$

Thus, using (40)-(41) the d-axis rotor flux can be calculated as follows:

$$\hat{\phi}_{dr}^e = \frac{L_{ag}}{1 + \tau_r s} i_{ds}^e, \quad (42)$$

where the magnitude of the flux can be controlled by controlling the i_{ds}^e in the form of a first-order low-pass filter (LPF) with a time constant $\tau_r = L_r/R_r$, which can be approximated by $\left|\hat{\lambda}_r\right| = \hat{\lambda}_{dr}^e \approx L_{ag} i_{ds}^e$.

The estimated torque equation is as follows $\hat{\phi}_{qr}^e = 0$:

$$T_m = \frac{3}{2}\frac{N_P}{2}\frac{L_{ag}}{L_r}\left(\hat{\phi}_{dr}^e i_{qs}^e - \hat{\phi}_{qr}^e i_{ds}^e\right)$$
$$= \frac{3}{2}\frac{N_P}{2}\frac{L_{ag}}{L_r}\left(\frac{L_{ag}}{1 + \tau_r s} i_{ds}^e\right) i_{qs}^e$$

$$\approx \frac{3}{2} \frac{N_P}{2} \frac{L_{ag}^2}{L_r} \left| \hat{\lambda}_r \right| i_{qs}^e. \tag{43}$$

Therefore, (43) shows that if the current in the dq-axis is controlled to be constant, the torque can be controlled to remain constant. Furthermore, when maintaining a constant magnitude of the dq current in the stationary frame, the dq current in the rotating coordinate frame also remains constant.

Proof: The dq-axis current is defined by $i_{ds}^e = i_{ds}^s \cos\theta_e + i_{qs}^s \sin\theta_e$, $i_{qs}^e = -i_{ds}^s \sin\theta_e + i_{qs}^s \cos\theta_e$. Thus, it can be expressed by the current of the stationary frame.

$$\left(i_{ds}^e \right)^2 + \left(i_{qs}^e \right)^2$$

$$= \left(i_{ds}^s \cos\theta_e + i_{qs}^s \sin\theta_e \right)^2 + \left(-i_{ds}^s \sin\theta_e + i_{qs}^s \cos\theta_e \right)^2$$

$$= \left(i_{ds}^s \right)^2 \cos^2\theta_e + 2i_{ds}^r i_{qs}^r \sin\theta_e \cos\theta_e + \left(i_{qs}^s \right)^2 \sin^2\theta_e$$

$$\quad + \left(i_{ds}^s \right)^2 \sin^2\theta_e - 2i_{ds}^r i_{qs}^r \sin\theta_e \cos\theta_e + \left(i_{qs}^s \right)^2 \cos^2\theta_e$$

$$= \left(i_{ds}^s \right)^2 + \left(i_{qs}^s \right)^2 \tag{44}$$

Thus, the soft starter employs the Park transformation of the three-phase current to regulate the firing angle, ensuring the constancy of the dq current. Fig. 6 shows the block diagram of the firing angle controller for the d-axis in the soft starter, where the parameters of the sampling and transport delay block can be determined by the soft starter. In Fig. 6, i_d^{ref} and i_d represent d-axis currents transformed from the ABC 3-phase currents through (36), with the same approach used to calculate the q-axis currents. Both the d-axis and q-axis currents are controlled using the same block diagram structure, although the calculation methods for the d-axis and q-axis currents are different. In the induction motor control system with a soft starter, the system pole is determined by the internal parameters of the induction motor, namely inductance and resistance. However, during the motor's startup, these internal parameters can double compared to their initial values [25]. Consequently, a current controller design method that accommodates these variations becomes essential.

This paper proposes a current controller design utilizing a Proportional-Integral (PI) controller. The advantage of employing a PI controller lies in increasing the system type and eliminating high-frequency noise, given that the soft starter acts as an LPF. Therefore, an LPF is generally applied with a cutoff frequency ranging from 1 to 3 kHz. The ideal approach to PI controller design involves setting the PI gain to cancel the pole of the induction motor. This ideal condition refers specifically to the concept of pole-zero cancellation, which aims to enhance system stability and performance by effectively achieving cancellation of the pole of the motor with the zero introduced by the PI controller. However, in real experimental systems, accurately determining the parameters based on the induction motor environment proves challenging. In this paper, the current controller is designed to function as an LPF. At first, the ideal case of the open-loop transfer function and closed-loop transfer function ($T_{\text{ideal}}(s)$) of the

controller can be expressed as follows:

$$G(s)P(s) = \frac{K_P \left(s + \frac{K_I}{K_P} \right)}{s} \left(\frac{\frac{1}{L}}{s + \frac{R}{L}} \right), \tag{45}$$

$$T_{\text{ideal}}(s) = \frac{G(s)P(s)}{1 + G(s)P(s)} = \frac{\frac{K_P}{L}}{s + \frac{K_P}{L}}. \tag{46}$$
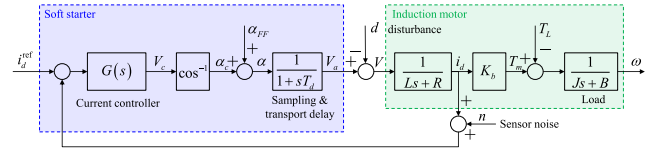

FIGURE 6. Block diagram of the firing angle controller.

where L represents the total inductance of the induction motor, R represents the total resistance of the induction motor, the ratio of the K_I/K_P is the same with R/L, and G(s) is the current controller ($G(s)$). However, in a real system, the ratio of the K_I/K_P and R/L couldn't be always the same. So, a real system of the closed-loop transfer function can be expressed as follows:

$$T_{\text{real}}(s) = \frac{\frac{K_P}{L} \left(s + \frac{C_\alpha}{\tau} \right)}{s^2 + \left(\frac{K_P}{L} + \frac{1}{\tau} \right) s + \frac{K_P}{L} \frac{C_\alpha}{\tau}}. \tag{47}$$

where C_α is the ratio of the K_I/K_P and R/L and τ is an electrical time constant of the induction motor. From (46), the distances of the poles and zero can be calculated as follows:

$$d_{1,2} = \left| -\frac{1}{2} \frac{K_P}{L} - \frac{1}{2\tau} \pm \frac{\sqrt{\left(\frac{K_P}{L} \right)^2 + \frac{2}{\tau} \frac{K_P}{L} + \frac{1}{\tau^2} - \frac{4C_\alpha}{\tau} \frac{K_P}{L}}}{2} \right.$$

$$\left. - \left(-\frac{C_\alpha}{\tau} \right) \right|. \tag{48}$$

Also, in an induction motor system, the τ is generally smaller than that of the control parameter $K_P/L(K_P/L \gg \tau)$, so the distances (47) can be simplified as follows:

$$d_1 = \left| -\frac{1}{2} \frac{K_P}{L} - \frac{1}{2\tau} + \frac{1}{2} \frac{K_P}{L} - \left(-\frac{C_\alpha}{\tau} \right) \right|. \tag{49}$$

From (48), d_1 indicates that the first pole and zero are very close, allowing them to cancel each other out, resulting in a non-dominant pole.

$$d_2 = \left| -\frac{1}{2} \frac{K_P}{L} - \frac{1}{2\tau} - \frac{1}{2} \frac{K_P}{L} - \left(-\frac{C_\alpha}{\tau} \right) \right|. \tag{50}$$

Conversely, d_2 shows the second pole is far apart from the zero, so the second pole is the dominant pole of the system. Thus, the first pole can be $-C_\alpha\tau$ and the second pole is K_P/L. Additionally, for a stable system, the control parameter K_P/L should satisfy the following constraint condition:

$$\frac{K_P}{L} > \frac{1}{(C_\alpha - 1)\tau - 1}. \tag{51}$$

Thus, the controller designed in this paper can serve as an LPF, functioning even when the exact parameters are unknown and considering the variation of the system pole.

Based on the analysis, a situation is assumed where the position of the pole changes from 5 to 10 during the induction motor's startup [25]. Initially, if zero is positioned to the left of the pole, the root locus during startup may appear as depicted in Fig. 7. In this scenario, setting the LPF in the 1 to 3 kHz band ensures that the conjugate pole does not occur, minimizing the impact on the control command and effectively eliminating high-frequency noise. Additionally, if the zero is to the right of the pole, the root locus can manifest as illustrated in Fig. 8 during startup. Despite the initial placement of zero on the left side of the pole, the situation may evolve as shown in Fig. 9, having no significant impact on the system response, and allowing the elimination of high-frequency noise. Thus, the current controller ($G(s)$) can be expressed as follows:

$$G(s) = K_P + \frac{K_I}{s} = \frac{K_P \left(s + \frac{K_I}{K_P} \right)}{s}, \qquad (52)$$

where the K_P is the proportional gain, and the K_I is the integral gain.

B. FIRING ANGLE CONTROL METHOD CONSIDERING THE AIR GAP VARIATIONS

As discussed in Session II, the air gap permeance is divided into mutual inductance and variable inductance. The mutual inductance of the air gap increases and becomes saturated as the rated speed is approached [25]. To maintain torque, it is necessary to reduce the current as compared to the initial start to account for this change in inductance. In this paper, considering this air gap changes, the firing angle reference is designed to ensure that the current magnitude decreases as the rated speed is approached. Initially, during the startup, the firing angle is held at a constant value until the d-axis current reaches a constant value. Subsequently, the firing angle is incrementally increased to reduce the current magnitude while considering the growing inductance. The feedforward firing angle control method is designed to increase the firing angle during startup, taking into account the characteristic of the air gap permeance that increases and then saturates near the rated speed. Therefore, it is possible to prevent a sudden increase in torque by increasing the firing angle based on modeling when the air gap permeance increases and then saturates. However, this proposed feedforward method estimates the changes in air gap permeance typically observed during the startup of induction motors based on the model, and it may not perfectly compensate for the variations in air gap permeance that differ among different induction motors. The proposed feedforward firing angle control method is as follows:

$$\alpha_0 = \begin{cases} \alpha_{init} & t < t_\alpha \\ \alpha_{init} + K_\alpha t_\alpha & t \geq t_\alpha \end{cases}, \qquad (53)$$

where t_α is the time until the d-axis current reaches a constant value, K_α is the firing angle gain, α_{init} and is the initial firing angle. The proposed feedforward method maintains the firing angle at an initial value during the period when the air gap permeance is increasing. After at least 60% of the startup time t_α, when the permeance begins to saturate, the firing angle is gradually increased [25]. The process for setting the firing angle parameters is detailed in Session IV.
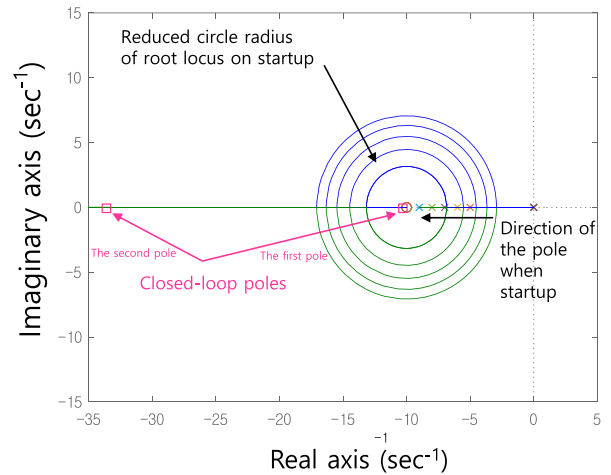

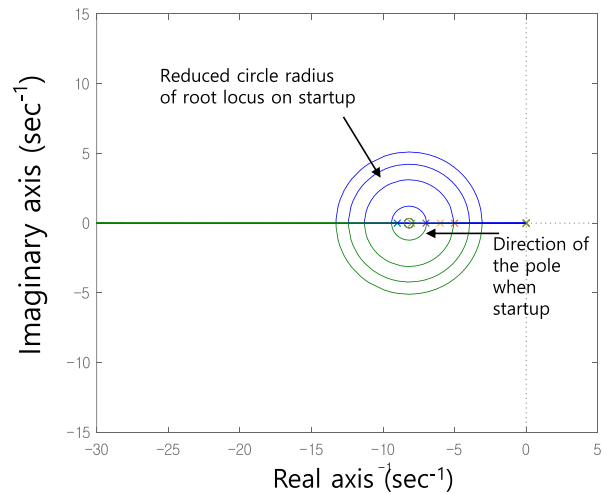**FIGURE 7.** Root locus of the induction motor startup (zero < pole).

FIGURE 8. Root locus of the induction motor startup (zero > pole).

IV. SIMULATION AND EXPERIMENTAL RESULTS

The proposed firing angle control method with less speed variation is simulated in MATLAB/SIMULINK, utilizing the induction motor model detailed in Session II. Genetic algorithms are favored for their capability to efficiently solve complex optimization problems. This methodology is utilized in various domains, including ion trap electrode estimation and induction motor parameter estimation, among others [26], [27]. The motor parameters for a double-squirrel cage induction motor are estimated using a genetic algorithm, based on datasheet information from an industrial induction motor as discussed in [26]. The block diagram of the
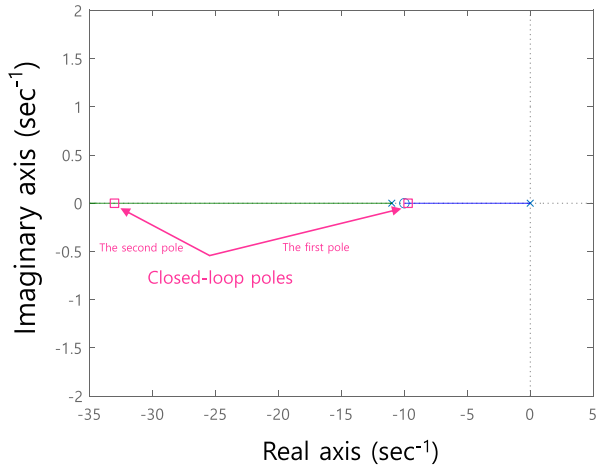
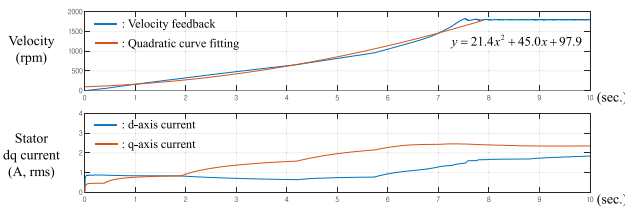**FIGURE 9.** Root locus of the induction motor startup when the pole is in the right side of the zero.

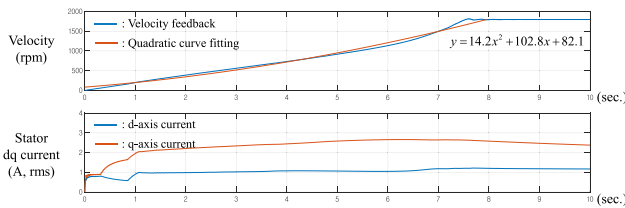**FIGURE 10.** Simulation result of the conventional voltage ramp-up method.

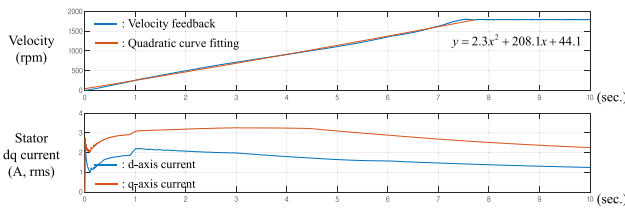**FIGURE 11.** Simulation result of the proposed method 1.

FIGURE 12. Simulation result of the proposed method 2.

TABLE 1. Parameters of the induction motor (blue: estimated parameters using a genetic algorithm).

Parameter	Value	Unit
Power	30	kW
Input voltage	380	V
Input frequency	60	Hz
Number of the poles	4	-
Rated speed	1765	rpm
Stator resistance	0.17	Ω
Stator leakage inductance	0.47	mH
Rotor resistance 1	0.10	Ω
Rotor resistance 2	0.91	Ω
Rotor leakage inductance 1	1.93	mH
Rotor leakage inductance 2	0.02	mH
Air gap mutual inductance	4.57	mH
Air gap variable inductance	8.71	mH

TABLE 2. Control parameters of the simulations.

Parameter	Conventional voltage ramp-up method	Proposed method 1	Proposed method 2
α_{init}	115°	115°	115°
K_{P}	-	0.5	0.5
K_{I}	-	0.1	0.1
K_{α}	-	-	0.8°/sec

TABLE 3. Parameters of the main induction motor.

Parameter	Value	Unit
Power	30	kW
Input voltage	380	V
Input frequency	60	Hz
Number of the poles	4	-
Rated current	59.8	A
Rated speed	1770	rpm
Load inertia	0.022	kg·m^2
Efficiency	94.1	%

TABLE 4. Parameters of the load induction motor.

Parameter	Value	Unit
Power	75	kW
Input voltage	380	V
Input frequency	60	Hz
Number of the poles	4	-
Rated current	148.7	A
Rated speed	1770	rpm
Load inertia	0.119	kg·m^2
Efficiency	90.7	%

induction motor system with a soft starter is illustrated in Fig.6. Table 1 lists the induction motor parameters, in which the variable inductance of the air gap accounts for 66% of the total air gap inductance. This air gap variable inductance significantly influences the total air gap inductance during the startup. The air gap mutual permeance refers to the permeance at the start of the operation, while the air gap variable inductance represents the varying values of air gap permeance during startup. The simulation employs three different methods: the conventional voltage ramp-up

method; proposed method 1, which maintains a constant dq current; and proposed method 2, which maintains a constant dq current while also accounting for air gap variations. For consistency between simulation and experimental settings, parameters such as the minimum firing angle set at 180/333°,

TABLE 5. Control parameters of the experiments.

Parameter	Conventional voltage ramp-up method	Proposed method 1	Proposed method 2
α_{init}	114˚	114˚	114˚
K_P	-	0.5	0.5
K_I	-	0.1	0.1
K_a	-	-	0.8˚/sec
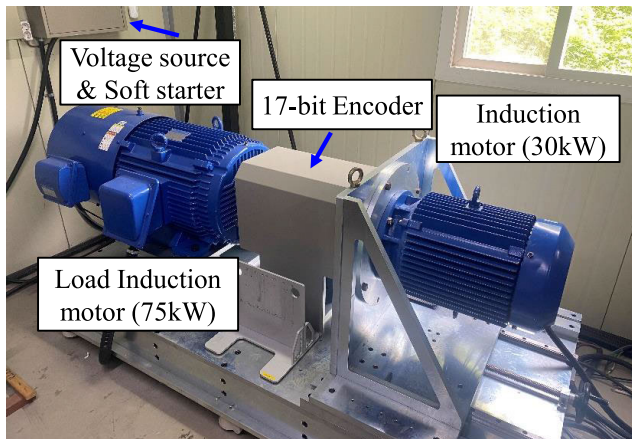
FIGURE 13. Experimental setup of the induction motor.

FIGURE 14. Experimental result of the conventional voltage ramp-up method.

FIGURE 15. Experimental result of the proposed method 1.

FIGURE 16. Experimental result of the proposed method 2.

the root mean square (RMS) current is also calculated with a 120 Hz sampling frequency, and a 7.5 second startup time are standardized. The simulation incorporates a load inertia of

119×10.3 kg·m^2 and employs a quadratic torque load type, typical of soft starter applications like centrifugal pumps and fans. Quadratic curve fitting applied to the speed data facilitated the assessment of speed variation, with a larger coefficient of the second-order term indicating greater variation. The control parameters are shown in Table 2 with the initial firing angles set for the same starting time. Fig. 10 shows the simulation result of the conventional voltage ramp-up method, with the coefficient of the second-order term being 21.4. Fig. 11 and Fig. 12 show the simulation results of the proposed methods 1 and 2, with the coefficient of the second-order term at 14.2 and 2.3, respectively. Applying the proposed method 1, which maintains a constant dq current, results in a 33.6% reduction in the coefficient of the second-order term, compared to the conventional voltage ramp-up method. Further enhancements are observed with proposed method 2, which accounts for air gap variation in addition to maintaining a constant dq current, achieving an 89.3% reduction in the coefficient of the second-order term. The experimental setup of the induction motor is shown in Fig. 13, which includes a 30kW induction motor (Higen motors, Korea) with a 17-bit resolution encoder (LS electric, Korea), and is paired with a 75kW induction motor (Higen motors, Korea) used as the load motor. The load motor is used to simulate real-world load conditions similar to those in applications such as fans and conveyor belts. Also, the three-phase voltage source is connected to the induction motor via the soft starter(Rockwell, USA), following the bond graph modeling approach. The inertia of the 30kW induction motor is 0.022 kg·m^2, and the inertia of the 75kW induction motor is 0.119 kg·m^2. The 75kW induction motor is used for heavy load conditions and possesses an inertia that is 5.4 times greater than that of the 30kW induction motor. The parameters of the main motor and load motor used in the experiments are detailed in Tables 3 and 4. Control parameters of the experiments are detailed in Table 5 with the initial firing angles set for the same starting times. Fig. 14 provides the experimental results utilizing the conventional voltage ramp-up method, demonstrating a coefficient of the second-order term at 32.3. This value serves as a baseline for comparing the effectiveness of the proposed control methods. Fig. 15 shows the experimental results of applying the proposed method 1, which maintains a constant dq current, resulting in a significantly reduced second-order term coefficient of 11.3. This reduction demonstrates the effectiveness of the proposed method 1 in mitigating speed variation during the startup. Fig. 16 shows the results from the proposed method 2, which not only maintains a constant dq current but also accounts for air gap variations. The second-order term coefficient is further reduced to 0.9, illustrating the substantial impact of considering air gap changes on enhancing motor startup performance. Hence, the experimental results show that proposed methods 1 and 2 result in reductions of the second-order term coefficient by 65.0% and 97.2%, respectively, when compared to the conventional voltage ramp-up method. Although the exact values of air gap permeance
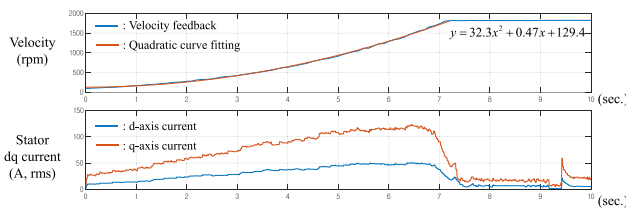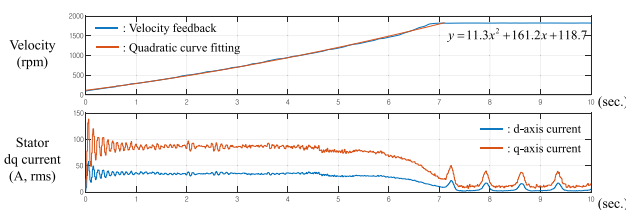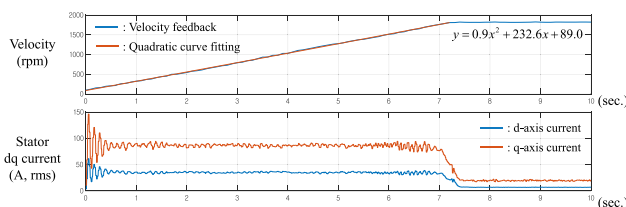
during changes cannot be measured in this experimental environment, the proposed method 2 effectively compensates for these changes through a feedforward control approach. This method demonstrated that the air gap permeance varied significantly before and after startup, and the feedforward control successfully compensated for these variations, ensuring improved performance during the motor startup phase. The experiments show reduced speed variation, although discrepancies between these results and the simulation findings might arise from inaccuracies in the induction motor modeling or the impact of temperature fluctuations during startup. Overall, both simulation and experimental results show that the proposed firing angle control method achieves improved starting performance, minimizing speed variation by adeptly accounting for air gap variation and current characteristics of the induction motor.

V. CONCLUSION

This paper developed a firing angle control method for soft starters to achieve a constant torque and a gradual speed increase, using only current feedback. In the startup phase of the induction motor, the air gap permeance was considered a state variable, but it had been utilized as a constant value in previous studies. Thus, the air gap permeance variation during motor startup was lumped as an effective inertia to model the transient response. The proposed control method effectively compensated for the change in air gap permeance during startup. This paper includes simulations of a 30kW induction motor, with parameters estimated using genetic algorithms and industrial motor data sheets. Experiments conducted with a 30kW industrial induction motor system demonstrated that, compared to the conventional voltage ramp-up method, the proposed method achieved a 97.2% reduction in the coefficient of the second-order term of the quadratic curve fitting of the speed. This reduction showed that the proposed method had improved starting performance with a smoother and more gradual increase in speed.

REFERENCES

[1] M. S. Mousavi, S. A. Davari, V. Nekoukar, C. Garcia, L. He, F. Wang, and J. Rodriguez, "Predictive torque control of induction motor based on a robust integral sliding mode observer," *IEEE Trans. Ind. Electron.*, vol. 70, no. 3, pp. 2339–2350, Mar. 2023.

[2] H. Wang, Y. Yang, X. Ge, Y. Zuo, Y. Yue, and S. Li, "PLL-and FLL-based speed estimation schemes for speed-sensorless control of induction motor drives: Review and new attempts," *IEEE Trans. Power Electron.*, vol. 37, no. 3, pp. 3334–3356, Mar. 2022.

[3] T. Wang, B. Wang, Y. Yu, and D. Xu, "Fast high-order terminal sliding-mode current controller for disturbance compensation and rapid convergence in induction motor drives," *IEEE Trans. Power Electron.*, vol. 38, no. 8, pp. 9593–9605, Aug. 2023.

[4] F. M. Bruce, R. J. Graefe, A. Lutz, and M. D. Panlener, "Reduced-voltage starting of squirrel-cage induction motors," *IEEE Trans. Ind. Appl.*, vol. IA-29, no. 1, pp. 46–55, Jan. 1984.

[5] G. Zenginobuz, I. Cadirci, M. Ermis, and C. Barlak, "Soft starting of large induction motors at constant current with minimized starting torque pulsations," *IEEE Trans. Ind. Appl.*, vol. 37, no. 5, pp. 1334–1347, Oct. 2001.

[6] T. A. Lipo, "The analysis of induction motors with voltage control by symmetrically triggered thyristors," *IEEE Trans. Power App. Syst.*, vol. PAS-90, no. 2, pp. 515–525, Mar. 1971.

[7] D. Gritter, D. Wang, and T. G. Habetler, "Soft starter inside delta motor modeling and its control," in *Proc. Conf. Rec. IEEE Ind. Appl. Conf. 35th IAS Annu. Meeting World Conf. Ind. Appl. Electr. Energy*, vol. 2, Aug. 2000, pp. 1137–1141.

[8] M. G. Solveson, B. Mirafzal, and N. A. O. Demerdash, "Soft-started induction motor modeling and heating issues for different starting profiles using a flux linkage ABC frame of reference," *IEEE Trans. Ind. Appl.*, vol. 42, no. 4, pp. 973–982, Jul. 2006.

[9] P. M. Shabestari and A. Mehrizi-Sani, "Current limiting and torque pulsation reduction of the induction motors," in *Proc. IEEE Power Energy Soc. Gen. Meeting (PESGM)*, Aug. 2019, pp. 1–5.

[10] S. Pandey, S. Bahadure, K. Kanakgiri, and N. M. Singh, "Two-phase soft start control of three-phase induction motor," in *Proc. IEEE 6th Int. Conf. Power Syst. (ICPS)*, Mar. 2016, pp. 1–6.

[11] D.-Y. Yang, T.-H. Kim, T.-H. Oh, Y.-S. Kim, S.-H. Lee, and D. D. Cho, "A current balancing method of two-phase soft starter for three-phase induction motor drive system without current sensor," in *Proc. 13th Asian Control Conf. (ASCC)*, May 2022, pp. 1309–1314.

[12] P. S. R. Nayak and T. A. Rufzal, "Flower pollination algorithm based PI controller design for induction motor scheme of soft-starting," in *Proc. 20th Nat. Power Syst. Conf. (NPSC)*, Dec. 2018, pp. 1–6.

[13] A. A. Menaem, M. Elgamal, A.-H. Abdel-Aty, E. E. Mahmoud, Z. Chen, and M. A. Hassan, "A proposed ANN-based acceleration control scheme for soft starting induction motor," *IEEE Access*, vol. 9, pp. 4253–4265, 2020.

[14] H. Nannen, H. Zatocil, and G. Griepentrog, "Novel predictive start-up algorithm for soft starter driven induction motors," in *Proc. IECON 46th Annu. Conf. IEEE Ind. Electron. Soc.*, Oct. 2020, pp. 3071–3078.

[15] H. Nannen, H. Zatocil, and G. Griepentrog, "Predictive firing algorithm for soft starter driven induction motors," *IEEE Trans. Ind. Electron.*, vol. 69, no. 12, pp. 12152–12161, Dec. 2022.

[16] J. S. Hsu and S. Member, "Monitoring of defects in induction motors through air-gap torque observation," *IEEE Trans. Ind. Appl.*, vol. 31, no. 5, pp. 1016–1021, Oct. 1995.

[17] B. U. Rai and L. Umanand, "Bond graph model of doubly fed three phase induction motor using the axis rotator element for frame transformation," *Simulation Model. Pract. Theory*, vol. 16, no. 10, pp. 1704–1712, Nov. 2008.

[18] H. A. Toliyat, M. S. Arefeen, and A. G. Parlos, "A method for dynamic simulation of air-gap eccentricity in induction machines," *IEEE Trans. Ind. Appl.*, vol. 32, no. 4, pp. 910–918, Aug. 1996.

[19] Y. Park, H. Choi, J. Shin, J. Park, S. B. Lee, and H. Jo, "Airgap flux based detection and classification of induction motor rotor and load defects during the starting transient," *IEEE Trans. Ind. Electron.*, vol. 67, no. 12, pp. 10075–10084, Dec. 2020.

[20] F. Blaschke, "The principle of field orientation-the basis for the transvector control of three-phase machines," *Siemens Zeitschrift*, vol. 45, no. 1, pp. 757–760, Jan. 1971.

[21] X. Wu, W. Huang, X. Lin, W. Jiang, Y. Zhao, and S. Zhu, "Direct torque control for induction motors based on minimum voltage vector error," *IEEE Trans. Ind. Electron.*, vol. 68, no. 5, pp. 3794–3804, May 2021.

[22] K. Hasse, "Zur dynamik drehzahlgeregelter antriebe mit stromrichter gespeisten asynchron-kuzschlublaufermachinen," Ph.D. dissertation, Techn. Hochschule Darmstat, Hesse, Germany, 1969.

[23] S. Karupusamy, M. A. Mustafa, B. M. Jos, P. Dahiya, R. Bhardwaj, P. Kanani, and A. Kumar, "Torque control-based induction motor speed control using anticipating power impulse technique," *Int. J. Adv. Manuf. Technol.*, vol. 124, pp. 1–9, Feb. 2023.

[24] R. S. C. Pal and A. R. Mohanty, "A simplified dynamical model of mixed eccentricity fault in a three-phase induction motor," *IEEE Trans. Ind. Electron.*, vol. 68, no. 5, pp. 4341–4350, May 2021.

[25] L.-C. Zai, C. L. DeMarco, and T. A. Lipo, "An extended Kalman filter approach to rotor time constant measurement in PWM induction motor drives," *IEEE Trans. Ind. Appl.*, vol. 28, no. 1, pp. 96–104, Feb. 1992.

[26] P. Pillay, R. Nolan, and T. Haque, "Application of genetic algorithms to motor parameter determination for transient torque calculations," *IEEE Trans. Ind. Appl.*, vol. 33, no. 5, pp. 1273–1282, Oct. 1997.

[27] M. Lee, Y. Park, S. Hong, C. Jung, T. Kim, Y. Kwon, and D. Cho, "Adjustment of replacement conditions for genetic algorithm used in optimizing ion-trap electrodes at a junction," in *Proc. 17th Int. Conf. Control, Automat. Syst. (ICCAS)*, Jeju, South Korea, Oct. 2017, pp. 1–6.

DAE-YOUNG YANG received the B.S. degree from the Department of Electronic Engineering, Tsinghua University, Beijing, China, in 2017. He is currently pursuing the Ph.D. degree with the Department of Electrical and Computer Engineering, Seoul National University, Seoul, South Korea. His research interests include the applications of power system control and nonlinear control theory to servo drive.

SANG-HOON LEE (Member, IEEE) received the B.S., M.S., and Ph.D. degrees in electrical and computer engineering from Seoul National University, Seoul, South Korea, in 1991, 1993, and 1997, respectively. He is currently a Research and Development Center Manager with RS Automation Company Ltd., Pyeongtaek, South Korea. His current research interests include nonlinear control theory and its application to electric machines and factory automation.

YOUNG-SEOK KIM received the B.S. degree from the Department of Electronic and Electrical Engineering, Sungkyunkwan University, Suwon, South Korea, in 2018. He is currently pursuing the Ph.D. degree with the Department of Electrical and Computer Engineering, Seoul National University, Seoul, South Korea. His research interests include the applications of nonlinear control theory to servo drive and sensors for motion control applications.

DONG-IL (DAN) CHO (Member, IEEE) received the Bachelor of Science degree from Carnegie Mellon University, USA, in 1980, and the Master of Science and Ph.D. degrees from Massachusetts Institute of Technology, USA, in 1984 and 1988, respectively. From 1987 to 1993, he was an Assistant Professor with the Department of Mechanical and Aerospace Engineering, Princeton University, USA. From 1993 to 2023, he was an Assistant Professor, an Associate Professor, and a Professor with the Department of Electrical and Computer Engineering, Seoul National University, South Korea. Since 2023, he has been the Chief Science Officer with RS Automation Company Ltd., South Korea. He has published over 150 journal articles and 150 patents. His research interests include nonlinear and intelligent control of robotic and mechatronic systems, MEMS-fabrication, and sensor technologies. He served as the President for ICROS and a BOG Member for IEEE CSS and EDS. He is the President of IFAC. He was elected as an Ordinary Member (2010–2012), a Senior Member (2013–2017, 2018–2023, and 2024), and a Senior Fellow (since 2024) of the National Academy of Engineering, South Korea. He served on the editorial board for many international journals, including the Co-Editor-in-Chief for *Mechatronics* (IFAC) and a Senior Editor for IEEE JOURNAL OF MICROELECTROMECHANICAL SYSTEMS.

TAE-HO OH received the B.S. and Ph.D. degrees in electrical and computer engineering from Seoul National University, Seoul, South Korea, in 2017 and 2023, respectively. His research interests include the applications of nonlinear control theory and machine learning algorithms to servo drive and sensors.

• • •